# Structural performance deterioration of corroding reinforced concrete columns in marine environments

*Hua-Peng Chen*[1*], *Yu Jiang*[1], *George Markou*[2]

([1]School of Transportation Engineering, East China JiaoTtong University, Nanchang, Jiangxi 330013, China;

[2]Department of Civil Engineering, University of Pretoria, Hatfield 0028, South Africa)

**Abstract**: In aggressive marine environments, rebar corrosion caused by chloride ion ingression in concrete is a critical factor leading to premature failure of in-service reinforced concrete (RC) structures. This paper investigated the structural performance deterioration of marine RC structures affected by rebar corrosion, and proposed new analytical models for predicting the residual bearing capacity of the corroded RC columns. By analyzing the performance deterioration mechanisms of the corroded RC structures, the material degradation models and structural strength reduction models were constructed. Then, the analytical models for estimating the residual bearing capacity of the corroded RC columns under various loading conditions were proposed. From the proposed models, the moment-axial force (M-N) interaction diagrams were plotted for analyzing the influence of corrosion damage locations on the residual bearing capacity. Furthermore, the impact of marine environmental factors on the service life of the corroding RC columns under various loading conditions was investigated. Finally, a numerical example for the corroded RC columns was given to demonstrate the effectiveness of the proposed models. The results showed that the residual bearing capacity of the marine RC columns can be significantly affected by the rebar corrosion level, corrosion damage location, load condition and in-service environment.

**Keywords:** Marine RC structure; Rebar corrosion; Concrete cracking; Residual bearing capacity; Remaining service life.

[*]Corresponding author.
E-mail: hp.chen@ecjtu.edu.cn; hp.chen@outlook.com (Hua-Peng Chen).

## 1. Introduction

In marine environments, reinforced concrete (RC) structures inevitably suffer from the ingression of harmful substances such as chloride ions, which deteriorates the safety and durability of marine concrete structures, leading to economic loss, resource wastes and even casualties. Research shows that rebar corrosion is the most fundamental factor responsible for the performance deterioration of marine concrete structures during the whole service life (Andrade et al., 2015; Balestra et al., 2019). Rebar corrosion consumes original materials, and generates much lighter rust products, resulting in the reduction in the yield strength and the loss in cross-sectional area of original rebar (Chen, 2018). With rebar corrosion development, the rust products continue to expand outward and produce a hoop tensile stress on the surrounding concrete, leading to the cracking in concrete and the deterioration of the bond strength between the rebar and the surrounding concrete (Zhang et al., 2019). After cracks connect each other, the concrete cover peels off (Yu et al., 2017), which causes further decrease in the rebar bond strength, and consequently affects the bearing capacity of the RC structures. Reinforcement corrosion not only reduces the reliability and safety of RC structures but also shortens the service life of the structures. Therefore, it is necessary to investigate the influence of rebar corrosion on the structural performance of marine concrete structures during their lifetime.

Extensive investigations have been undertaken during the last decade regarding the effects of reinforcement corrosion on the performance of RC structures (Chen and Xiao,2012; Zhu and Francois, 2014; Yu et al., 2015; Chen and Nepal, 2018). Many experimental studies were conducted to assess the influence of rebar corrosion on concrete cracking, and the results showed that the crack width develops as rebar corrosion progresses (Vidal et al., 2004; Val et al., 2009; Coronelli et al., 2013; Khan et al., 2014). The process of corrosion-induced concrete cracking can be divided into three phases, including crack initiation, crack propagation, and fully concrete cover loss (Chen and Alani, 2013). Then, the analytical model was proposed for predicting the corrosion-induced concrete crack width growth, based on the elasticity theory and fracture mechanics. In addition, studies showed that rebar bond strength may increase at the early stage of rebar corrosion and then deteriorate rapidly to a low value

after cracks appear on concrete cover surface (Fischer, 2010; Law et al., 2011; Li and Yuan, 2013). The combined action of rebar corrosion and concrete cracking may cause the incompatibility of the stress-stain relationship between the rebar and the surrounding concrete (Coccia et al., 2016). Moreover, as the unconstrained length of the corroded rebar inside the RC columns increases, the compressed steel bars are prone to buckling in advance (Tapan and Aboutaha, 2011). In order to balance the decrease in rebar bearing capacity and the loss of the concrete cross-section, the compression zone height of the concrete cross-section may change. Therefore, these factors caused by rebar corrosion, including concrete cracking and rebar bond failure, affect the lifetime performance of RC structures.

The residual bearing capacity of the corroded RC structures has also been investigated in many studies (Wang and Liang, 2008; Tapan and Aboutaha, 2011; Dang and François, 2013; Dong et al., 2016). Chen (2018) evaluated the load-carrying capacity deterioration of the corroded concrete beam by considering many crucial factors, including the loss of rebar cross-section and yield strength, concrete cracking, and rebar bond strength degradation. The results showed that the rebar bond strength degradation may change the structural failure mode of the corroded concrete beams. By conducting the accelerated corrosion tests on circular columns, Ma (2012) investigated the degradation of the seismic performance of the corroded RC columns, and proposed an empirical model for predicting the residual bearing capacity of the corroded columns. Meda (2014) evaluated the influence of longitudinal rebar corrosion on the cyclic behavior of RC columns through two full-scale cyclic tests. Yalciner (2019) conducted an experimental study for predicting the seismic performance levels of the corroded RC columns as a function of the initial corrosion crack width, and then developed empirical models suitable for on-site structural evaluation. Based on the experimental results of full-scale RC columns, Yalciner (2020) developed an empirical model for predicting the structural behavior of the corroded RC columns. Tapan and Aboutaha (2011) considered many effects to predict the residual bearing capacity of the corroded RC columns under different degradation conditions, such as the rebar yield strength decrease and cross-section reduction, rebar buckling, and deformation incompatibility between the rebar and the surrounding concrete. Dang and François (2013) analyzed the effect of rebar corrosion on the flexural behavior of the corroded RC beams and further predicted the residual flexural

strength of the concrete beams. In addition, by controlling the corrosion level and the length of the corroded area, experiments were carried out to test the bearing capacity of corrosion-damaged eccentrically loaded RC columns. The results indicated that the bearing capacity of RC columns with small eccentricity decreased significantly by the corroded steel bars in the compression zone, and in the case of the corroded columns with large eccentricity, a greater reduction of load capacity was shown in the columns with the corroded rebar on the tensile side. Consequently, as corrosion progresses, many key factors influence the residual bearing capacity of the corroded RC structures, such as rebar bearing capacity reduction, rebar bond failure, concrete cracking, and change in concrete compression zone height. Therefore, in order to assess the residual bearing capacity of the corroded RC columns, the degradation of rebar and concrete material properties and the loss of the structural strength need to be considered in calculations. However, in the existing studies on the residual bearing capacity of the corroded RC columns, many critical factors were not quantitatively investigated, such as the reduction of concrete cross-sectional area and the change in the compression zone height of the concrete cross-section. Thus, it is necessary to carry out in-depth investigations on the residual bearing capacity of the corroded RC columns to estimate the remaining service life of the structures subjected to marine environments.

In this paper, the material degradation models and the structural strength reduction models were proposed based on the analysis of the material damage mechanisms caused by rebar corrosion. The analytical models for predicting the residual load-bearing capacity of the corroded RC columns were provided. The moment-axial force (M-N) interaction diagrams of the corroded columns were obtained for different cases with rebar corrosion levels and damage locations. The service life of the corroded RC columns in various aggressive environments was also estimated. Finally, a numerical example was adopted to demonstrate the effectiveness of the proposed analytical models by comparing the predicted results with the available experimental data.

## 2. Rebar and concrete material degradation models

In RC structures, the concrete material is highly alkaline. After hydration reaction, a thin passivation film is formed on the surface of the steel bar, thus the steel bar could resist corrosion in a relatively neutral and acidic environment (Zhu and Francois, 2014). However, in the marine environment, chloride ion ingress into the concrete occurs during the construction and in-service phases, leading to damage in the steel bars in the weakened areas of the passive film, causing corrosion of the steel bars in the RC structures, and finally resulting in reduction in bearing capacity of the structures. Figure 1 shows the underlying mechanisms for the bearing capacity reduction of the corroded RC columns.

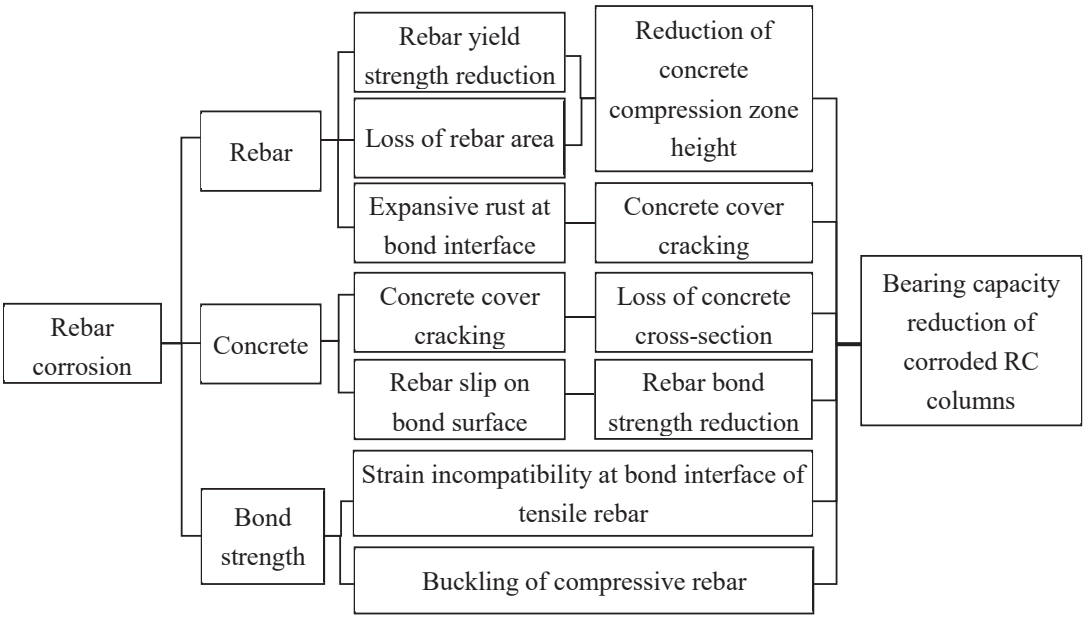


**Figure 1** Material damage mechanisms and bearing capacity reduction caused by rebar corrosion

## 2.1. Reinforcement corrosion

The initial occurrence of rebar corrosion induced by chlorides in marine environments could be corrosion pits, but rebar corrosion could become approximately uniform with increase in corrosion level (Balestra et al., 2019). As rebar corrosion progresses, the yield strength and the cross-sectional area of the corroded rebar decrease gradually. At the earlier corrosion stage, the residual bearing capacity of the yielding rebar $F_{sc}$ can be given by

$$F_{sc} = f_{yc} A_{sc} \tag{1}$$

At the corrosion level $X$, the residual yield strength of the corroded rebar $f_{yc}$ can be estimated from $f_{yc}=(1-\gamma X)f_{y0}$, and the residual area of the corroded rebar $A_{sc}$ can be calculated from $A_{sc}=(1-X)A_0$, in which $\gamma$ is the influence coefficient of nonuniform corrosion estimated from experiments (Du et al., 2005), taken here as 0.5, $f_{y0}$ is the yield strength of the uncorroded rebar, and $A_0$ is the area of the uncorroded rebar. For the corroded RC structures, the corrosion level $X$ is typically expressed by the ratio between the consumed mass of the corroded steel bar $\Delta m_s$ and the original mass of the steel bar $m_0$, defined here as

$$X = \frac{\Delta m_s}{m_0} = \frac{\Delta A_s}{A_0} \tag{2}$$

where $\Delta A_s$ is the loss of the cross-sectional area of the corroded rebar. Meanwhile, rebar corrosion level largely depends on the condition of aggressive environments, and the relationship between the corrosion level $X$ and the mean annual corrosion current per unit length at the surface area of the rebar $i_{corr}$ (A/m$^2$) can be determined from

$$X = 4\frac{x_{corr}}{D_b} = m_c \frac{i_{corr} t}{D_b} \tag{3}$$

where $t$ is the duration of corrosion (year); $D_b$ is the diameter of the intact rebar (m); $x_{corr}$ is the corrosion attack penetration (m); and $m_c$ is a dimensionless empirical coefficient, taken as $m_c=4.6\times10^{-3}$. With the increase of the corrosion level, the volume of the corrosion products expands continuously at the rebar bond interface. Due to different types of corrosion products, the volume of corrosion products can range from 2 to 6 times the volume of the original steel bar consumed (Chen and Nepal, 2018). The volume expansion factor $\xi_r=A_r/\Delta A_s$ is then introduced to represent the ratio of the volume of corrosion products per unit length $A_r$ to the original rebar area loss $\Delta A_s$. From Eq. (2), the rust volume per unit length over time $A_r$, associated with the rebar corrosion level $X$, is expressed as

$$A_r(t) = M_r / \rho_r = \xi_r X A_0 \tag{4}$$

where $M_r$ is the mass of rust in kg/m, and $\rho_r$ is the density of corrosion rust with an approximate value of $\rho_r$=3600 kg/m$^3$. In addition, to accommodate the increase in volume per unit length $\Delta V_r=A_r-\Delta A_s=(\xi_r-1)\Delta A_s$, the radial displacement at the bond interface $\bar{u}_b$ is generated (Chen, 2018), given as

$$\bar{u}_b(X) = \Delta V_r / (\pi D_b) = (\xi_r - 1) D_b X / 4 \tag{5}$$

Since the thickness of the rust layer $t_r$ is much smaller than the uncorroded rebar radius $R_b$, the thickness of the rust layer $t_r$ can be estimated by the ratio of the rust volume per unit length $A_r$ over the perimeter of the original rebar, taken as $t_r=A_r/2\pi R_b$. The corrosion penetration rate $t_r/R_b$, defined as the ratio of the thickness of the rust layer over the original rebar radius $R_b$, could be then expressed as

$$\frac{t_r}{R_b}=\frac{M_r}{2\pi R_b^2\rho_r}=\frac{\xi_r}{2}X \tag{6}$$

### 2.2. Concrete cracking

The crack width on the concrete cover surface is an important factor for estimating the load-carrying capacity of the corroded RC structures. The rebar-concrete model based on the thick-walled cylinder theory has been frequently adopted to analyze cover concrete cracking evolution (Liang and Wang, 2020), and can be considered as an axisymmetric plain-stress problem due to the assumed uniform expansion, as shown in Figure 2.

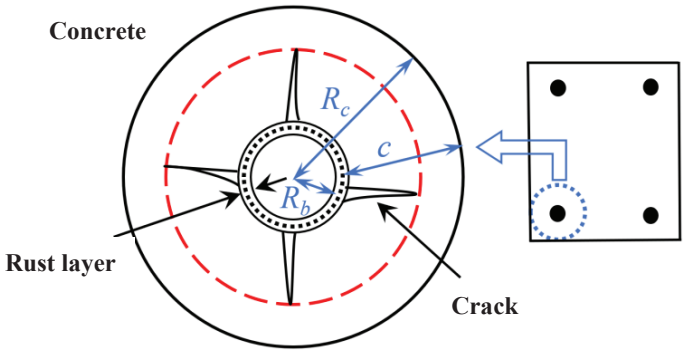


**Figure 2** Concrete cover cracking evolution model caused by rebar corrosion

The corrosion-induced concrete cracking process could be considered as an anisotropic nonlinear elastic problem, and the bilinear stress softening curve of cohesive cracking concrete was adopted to quantify crack propagating in the concrete cover (Chen and Xiao, 2012). In the bilinear stress softening curve, the residual tensile stress in hoop direction $\sigma_\theta$ for the cracked concrete could be expressed as

$$\sigma_\theta=\sigma_w=f_t(a-bW) \tag{7}$$

where $\sigma_w$ is the residual tensile stress crossing cohesive cracks; $f_t$ is the tensile strength of the intact concrete; $W$ is the dimensionless variable that normalizes actual crack width $w(r)$ to a

non-dimensional form, defined as $W=f_t w(r)/G_f$, in which $G_f$ is the fracture energy of the concrete; coefficients $a$ and $b$ depend on the stage of crack width, including pre-critical stage ($0 \le W \le W_{cr}$) and post-critical stage ($W_{cr} \le W \le W_u$), given by

$$a = a^{cr} = 1; b = b^{cr} = \frac{1-\alpha_{bi}}{W_{cr}} \quad \text{for pre-critical stage} \tag{8a}$$

$$a = a^{u} = \frac{\alpha_{bi} W_u}{W_u - W_{cr}}; b = b^{u} = \frac{\alpha_{bi}}{W_u - W_{cr}} \quad \text{for post-critical stage} \tag{8b}$$

where $W_{cr}$ is the normalized value of the critical crack width $w_{cr}$; $W_u$ is the normalized value of the ultimate cohesive crack width $w_u$, which can be evaluated from the maximum aggregate size of concrete materials; and coefficient $\alpha_{bi}$ is given as $\alpha_{bi}$ =0.15 (CEB-FIP, 1990). By using the general solution of normalized crack width and boundary conditions, the normalized crack width $W_b$ at the bond interface can be given as

$$W_b = \frac{1}{b(l_0 - R_b)} \left(\frac{E}{f_t} \bar{u}_b - a R_b\right) \tag{9}$$

where $l_0=n_c l_{ch}/(2\pi b)$ (CEB-FIP, 1990), in which $n_c$ is the total number of the cracks in the cover estimated from $n_c \approx 2\pi R_c/L_c$ (Zhang et al., 2010), and spacing of crack bands $L_c$ is approximately three times the maximum aggregate size; $R_c=R_b+c$, in which $c$ is the concrete cover thickness; $l_{ch}$ is characteristic length taken as $l_{ch}=EG_f/f_t^2$, in which $E$ is the modulus of elasticity for intact concrete.

When the crack width at the bond interface is smaller than the critical value ($W_b \leqslant W_{cr}$) and the crack front reaches the concrete cover surface, the normalized crack width $W_b^{cr}$ at the bond interface can be calculated from

$$W_b^{cr} = (1+v) R_c (l_0^{cr} - R_c)(\delta(l_0^{cr}, R_c) - \delta(l_0^{cr}, R_b)) \frac{W_{cr}}{1-\alpha_{bi}} \tag{10}$$

where $v$ is Poisson's ratio; $l_0^{cr}$ is the material coefficient determined by the general coefficient $l_0$ by using $b=b^{cr}$; the crack width coefficient $\delta(l_0, r)$ is defined as

$$\delta(l_0, r) = \frac{1}{l_0 (l_0 - r)} - \frac{1}{l_0^2} \ln \frac{|l_0 - r|}{r} \tag{11}$$

and coefficients $\delta(l_0^{cr}, R_c)$ and $\delta(l_0^{cr}, R_b)$ are determined by the general coefficient $\delta(l_0, r)$, in which $l_0=l_0^{cr}$, $r=R_c$ and $r=R_b$, respectively. When crack width at the bond surface exceeds the critical value ($W_b > W_{cr}$) and the crack front reaches the concrete cover surface, the normalized crack width $W_b^u$ at the bond interface (Chen and Xiao, 2012) can be calculated from

$$W_b^u = W_{cr} + \frac{(1-\alpha_{bi})}{\alpha_{bi}} \frac{(l_0^u - r_{cr})}{(l_0^{cr} - r_{cr})} \frac{[\delta(l_0^u, R_b) - \delta(l_0^u, r_{cr})]}{[\delta(l_0^{cr}, r_{cr}) - \delta(l_0^{cr}, R_c)]} (W_u - W_{cr}) \tag{12}$$

where material coefficient $l_0^u$ is determined by the general coefficient $l_0$ in which $b=b^u$, and the critical crack boundary $r_{cr}$ can be obtained from

$$(1+v)R_c(l_0^{cr} - R_c)(\delta(l_0^{cr}, R_c) - \delta(l_0^{cr}, r_{cr})) = (1-\alpha_{bi}) \tag{13}$$

In the calculations, the radial displacement at the bond interface $\bar{u}_b$ then can be calculated from Eq. (9) in different cases, and the corresponding critical corrosion penetration $t_{cr}$ can be obtained from Eq. (6).

After cracks appear on the concrete cover surface, the rebar bond strength degradation and the concrete section area reduction may have significant influence on the bearing capacity of the corroded RC columns. Thus, it is necessary to investigate the relationship between the corrosion level $X$ and the crack width on the concrete cover surface. When cracks reach the surface of the concrete cover, by considering free surface condition at the concrete cover surface and ignoring the Poisson's effect associated with the hoop strain of the completely cracked concrete (Chen and Xiao, 2012), the normalized crack width on the concrete cover surface $W_c$ as a function of the corrosion level $X$ can be obtained from

$$W_c = \frac{W_u(\frac{E}{f_t}\frac{R_b X}{2}(\xi_r - 1)(\frac{W_u - W_{cr}}{\alpha_{bi} W_u}) - R_b - (l_0^u - R_b)\Delta_{cb})}{(l_0^u - R_b)(1-\Delta_{cb})} \tag{14}$$

where the crack coefficient $\Delta_{cb}$ is defined as

$$\Delta_{cb} = R_c(l_0^u - R_c)(\delta(l_0^u, R_c) - \delta(l_0^u, R_b)) \tag{15}$$

Finally, the equivalent crack width wc is defined as the cumulated crack width at the concrete cover surface, calculated from $w_c = W_c G_f / f_t$. The process of concrete cracking continues until crack width reaches the ultimate cohesive value. The corrosion level at the time when the equivalent crack in the concrete cover reaches its ultimate cohesive value can be obtained from

$$X_u = \frac{W_u}{(\xi_r - 1)} \frac{f_t}{E} \frac{n_c l_{ch}}{\pi R_b} \tag{16}$$

After crack width reaches the ultimate cohesive value, the cracking in the concrete cover becomes discrete. The width of concrete cracks could continue to increase due to the progressive expansion of the corrosion rust layer at the rebar bond interface, by assuming that

no rust enters the spaces in cracks. The average increase of the width in the individual crack within the cover concrete after the ultimate cohesive crack width can be determined from the increase of the perimeter of the front of the corrosion products (Chen and Alani, 2013).

### 2.3. Concrete cross-section loss

Although the concrete cover may not directly peel off immediately after cracks appear on the concrete surface, the concrete cover with cracks can cause serviceability issues before the structure reaches its ultimate bearing capacity. Thus, it is essential to consider the effect of the loss of concrete cross-section areas on the ultimate capacity of the corroded RC structure. In this paper, the damaged concrete cross-sectional area of the corroded column is simplified by adopting the equivalent rectangular cross-section, as shown in Figure 3(b).

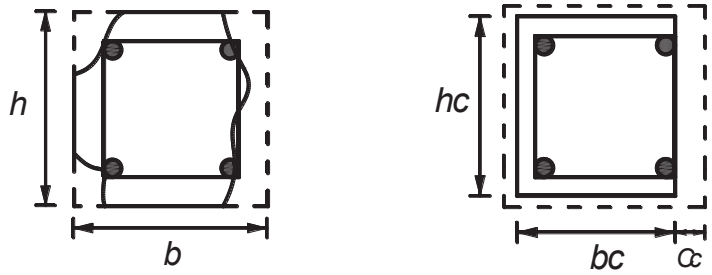


(a) Potential damage of concrete cross-section

(b) Simplified diagram of damaged cross-section

**Figure 3** Damage in concrete cross-sectional area of corroded RC columns

By considering the experimental data of the concrete cross-section damage (Hui et al., 1997) and the crack width of the concrete surface $w_c$, the loss of the concrete cross-section areas due to the rebar corrosion can be estimated. The residual size of the corrosion-damaged concrete cross-section is given here as

$$c_c = \min(c\frac{w_c}{T}, c) \tag{17}$$

$$b_c = b - c_l - c_r \quad ; \quad h_c = h - c_u - c_d \tag{18}$$

where $c_c$ is the loss of the concrete cover thickness after corrosion damage; $T$ is estimated from the load-carrying capacity test of the corroded RC column, which is the total crack width on the concrete surface when the concrete cover is completely spalling, taken here as

$T$=0.003m (Hui et al., 1997); $h$ and $b$ are original depth and width of the concrete cross-section, respectively; $h_c$ and $b_c$ are residual depth and width of the corrosion damaged concrete cross-section, respectively; $c_l$, $c_r$, $c_u$ and $c_d$ are the loss of the concrete cover thicknesses on the left, right, upper and lower sides of the concrete cross-section, respectively. The loss of the concrete cross-section can cause the change in the height of the concrete compression zone.

## 3. Structural strength degradation models

### 3.1. Rebar bond degradation

The bond strength between the rebar and intact concrete ensures that the RC structure can fully bear the design load. When the rebar bond strength degrades, the force cannot be transferred effectively between the rebar and the surrounding concrete, resulting in the deterioration of the structural performance and the decrease of the structural bearing capacity. For the corroded RC members, the stirrups partly prevent the cracking and spalling of the concrete cover (Saatcioglu and Razvi, 1992), and also increase the friction force between the corroded rebar and the surrounding concrete by inhibiting the lateral deformation. However, the corrosion of stirrups can be more serious than that of longitudinal rebar in general, which may make limited contributions to the residual bound strength of the corroded rebar (Wang and Liang, 2008). When the confining stresses in concrete and stirrups are not available, the effect of the confinement by stirrups on rebar bond strength can be considered by introducing coefficient $\boldsymbol{\lambda_\eta}$, and the residual bond strength can be simply estimated from concrete crack width (Cairns et al., 2006; Chen, 2018), expressed here as

$$\zeta(X) = D_b / (D_b + \lambda_\eta w_c(X)) \tag{19}$$

where $\zeta(X)$ is the residual bond strength ratio, and coefficient $\lambda_\eta$ is estimated from rebar bond strength experiments, taken as $\lambda_\eta$=15~20 (Cairns et al., 2006). Then, the residual bond strength $\tau_{ux}$ can be obtained by calculating the ultimate bond strength of the rebar with intact concrete $\tau_{u0}$, namely

$$\tau_{ux}(X) = \zeta(X)\tau_{u0} \tag{20}$$

For RC columns with a relatively high corrosion level, insufficient bond strength may lead to a change in the failure mode of the steel bars. When rebar anchorage fails, the bearing capacity of the rebar with bond deterioration $F_{ux}$ can be determined by the residual bond strength. The load-carrying capacity of the corroded rebar then can be rewritten from Eq. (1) as

$$F_{ux} = \pi D_c l_{dc} \tau_{ux}(X) \tag{21}$$

where $D_c$ is the residual diameter of the corroded rebar, calculated from $D_c=D_b(1-X)^{0.5}$; the development length of the corroded rebar $l_{dc}$ can be determined from $l_{dc}=\delta l_d$, where $l_d$ is the design development length, calculated from $l_d=a_{bd}D_b f_{yd}/4f_{bd}$, in which $f_{yd}$ is the design strength of the tensile rebar, $f_{bd}$ is the design bond strength obtained from concrete strength, $a_{bd}$ is the coefficient depending on many factors including the shape of anchorage, the type of confinement provided by the stirrups and concrete cover; and the residual development length ratio $\delta$ is determined by the linear fitting of experimental results (Chung et al., 2004), expressed here as

$$\delta = \begin{cases} 0.968 - 0.210X & X \geq 0.02 \\ 1.0 & X \prec 0.02 \end{cases} \tag{22}$$

Consequently, the residual bearing capacity of the corroded rebar after bond failure can be obtained on the basis of the equivalent distribution of the bond stress along the development length (Chiu et al., 2014), where the effect of rebar slip on the residual bearing capacity is also considered.

When the rebar bond strength is intact, the strain of the rebar $\varepsilon_{sx}$ is equal to the strain of the concrete $\varepsilon_{sc}$. However, when the rebar bond is damaged, the corroded rebar may slip due to loading, resulting in the inconsistent stress-strain relationship between the rebar and the surrounding concrete, i.e., the strain of the surrounding concrete $\varepsilon_{sc}$ is greater than the strain of the rebar $\varepsilon_{sx}$. Here, the interpolation factor $G(X)$ is introduced to establish a new deformation coordination equation between the rebar and concrete after bond loss (Wang and Liu, 2009), expressed here as

$$G(X) = \frac{L_{eq}}{L_{ub}} = \frac{2L_{soft}}{L_{ub}} = \frac{2(\varepsilon_{end} - \varepsilon_{start})Y_x(X)}{\tan(17.5^\circ)\varepsilon_{end} L_{ub}} \tag{23}$$

where $L_{eq}$ is the length of the equivalent plastic section (Daniell et al., 2008); $L_{soft}$ is the length of the equivalent softened section; $L_{ub}$ is the unbonded length of the tensile steel bar; $Y_x$ is the compression zone height of concrete cross-section; and the initial and final strains

could be taken as $\varepsilon_{start}$=0.002 and $\varepsilon_{end}$=0.006, respectively (Ho et al., 2004). Thus, the strain relationship between the steel bar and the concrete becomes $\varepsilon_{sx}= G(X)\varepsilon_{sc.}$

### 3.2 Buckling of corroded compressive rebar

Under the combined action of more severe stirrup corrosion and the concrete cover cracking, the longitudinal unbraced length of the rebar increases, the instability of the longitudinal steel bar before reaching its yield strength therefore should be considered. After rebar bulking, the critical buckling stress $f_{cr}$ can be obtained by using Euler's formula, expressed here as

$$f_{cr} = \pi^2 E_{sc} I_{sc} / (L_{exp}^2 \cdot A_{sc}) \tag{24}$$

where $E_{sc}$ is the elastic modulus of the corroded longitudinal bars, and the initial value $E_s$ can be taken, since rebar corrosion has no obvious effect on the elastic modulus; the inertia moment of the corroded reinforcement $I_{sc}$ is calculated from $I_{sc}=\pi D_c^4/64$; $L_{exp}$ is the laterally unbraced length of the structural member given as $L_{exp}=n_r s$, in which $s$ is the stirrup spacing; and $n_r$ is the order of the compressed longitudinal rebar, when the deformation of the corroded steel bar crosses ($n$-1) stirrups.

## 4. Residual bearing capacity

### 4.1 Columns in axial compression ($e$=0)

In the case of RC columns under axial compression (i.e., eccentricity $e$=0), the entire cross-section of the RC column is compressed, including all steel bars. By considering the stress state of the RC column under concentric loading and the degradation models of material and structural strength, the residual bearing capacity of the corroded rebar can be obtained, expressed here as

$$F_{szx} = \min(f_{cr}, f'_{yc}) A'_{sc} \qquad \text{for near loading side} \tag{25}$$

$$F_{sx} = \min(f_{cr}, f_{yc}) A_{sc} \qquad \text{for far loading side} \tag{26}$$

where $F_{szx}$ and $F_{sx}$ are the bearing capacity of the rebar on the near and far sides of loading, respectively, which can be determined by the smaller value of the rebar yield strength and buckling strength; and $f'_{yc}$ and $A'_{sc}$ are the residual yield strength and cross-sectional area of

the corroded rebar on the side closer to the load, respectively. Meanwhile, the residual bearing capacity of the concrete $F_{cx}$ can be calculated from

$$F_{cx} = a_1 h_c b_c f_c \tag{27}$$

where $a_1$ is the coefficient taken as unity (CEB-FIP, 1990); $h_c$ and $b_c$ are residual depth and width of the concrete cross-section after concrete cover spalling, calculated by Eq. (18), respectively; and $f_c$ is the concrete compressive strength. Finally, the bearing capacity of the corroded RC column under axial loading $N$ is given by

$$N(X) = F_{cx} + F_{szx} + F_{sx} \tag{28}$$

### 4.2 Columns in eccentric compression

In the cases of RC columns under eccentric loading, structural members are subjected to the combined action of axial load and bending moment. Figure 4 shows the geometry, force and strains of the typical cross-section of the corroded RC column.

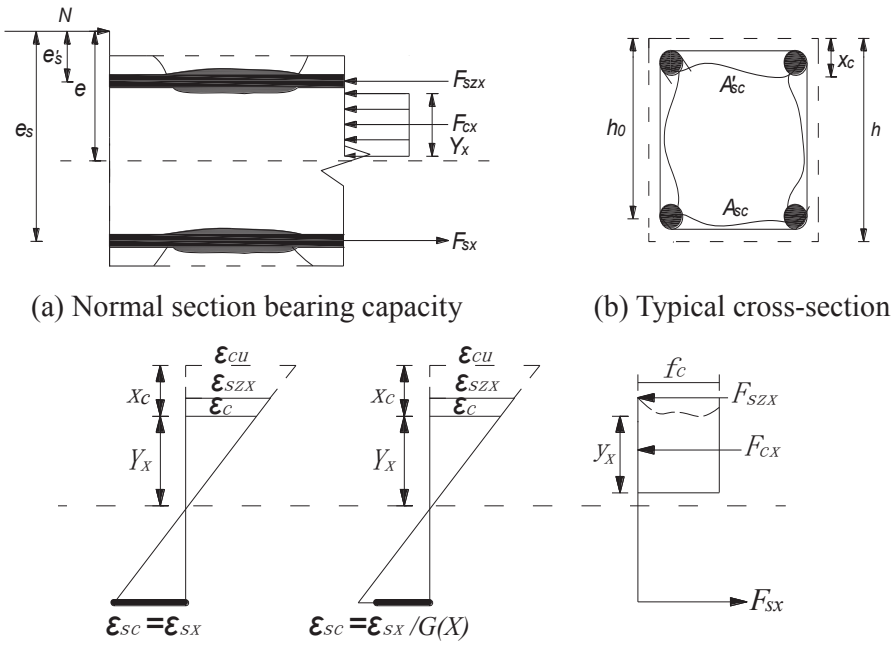


(a) Normal section bearing capacity (b) Typical cross-section

(c) Strain distribution with effective bond (d) Strain distribution at bond failure (e) Equivalent stress distribution

**Figure 4** Applied forces and stress distribution diagram of the normal cross-section of the corroded RC column and parameter definitions

In Figure 4, $e'_s$ and $e_s$ are the distances from the loading location to the centroid of the rebar on the side close to the load and away from the load, respectively; the distance $e_s$ is expressed as $e_s=e+h/2-a_s$; $e$ is the eccentricity of the applied load defined as $e=e_0+e_a$, in which $e_0$ is the load eccentricity and $e_a$ is the additional eccentricity; $Y_x$ is the compression zone height of the concrete column obtained from $Y_x=\beta_1 y_x$, in which $\beta_1$ is the coefficient taken here as 0.9 (CEB-FIP, 1990); $y_x$ is the equivalent compressive zone of the concrete; $h_0$ is the effective depth of column given by $h_0=h-a_s$, in which $a_s$ is the distance from the centroid of the rebar on the far side of loading to the edge of concrete cover; $x_c$ is the average loss of the concrete height in the compression zone taken as $x_c=c_u$, in which $c_u$ is calculated from Eq. (17); $\varepsilon_{szx}$ and $\varepsilon_{sx}$ are the strains of the rebar on the near and far sides of loading, respectively; $\varepsilon_{sc}$ is the strain of the concrete away from loading; $\varepsilon_c$ is the strain of compressive concrete ($\varepsilon_c \leq \varepsilon_{cu}$); and $\varepsilon_{cu}$ is the ultimate compressive strain of the concrete (CEB-FIP, 1990).

For eccentrically loaded RC columns, the failure types can be divided into two groups, i.e. the large eccentric compression failure and small eccentric compression failure. Similarly, by combining the degradation models of material and structural strength with the equilibrium conditions of the resultant forces acting on the corroded column section, the residual bearing capacity of the corrosion-damaged eccentrically loaded columns can be calculated from

$$N = a_1 \beta_1 b_c f_c Y_x(X) + F_{szx} - F_{sx} \tag{29a}$$

$$N \cdot e_s = a_1 \beta_1 b_c f_c Y_x(X)(h_0 - x_c - \frac{\beta_1 Y_x(X)}{2}) + F_{szx}(h_0 - a'_s) \tag{29b}$$

where $a'_s$ is the distance from the centroid of the rebar on the near side of loading to the edge of the concrete cover. For the corroded RC columns, the residual bearing capacity of the concrete cross-section needs to be calculated on the basis of the growth of the concrete cracks, and the bearing capacity of the corroded rebar needs to be determined, depending on the rebar stress state (in tension or in compression), rebar bond effectiveness, and rebar buckling occurrence. Based on the actual stress status of the steel rebar and the degradation models described above, the residual bearing capacity of the rebar under various loading conditions can be determined accordingly, as described below in detail.

**4.2.1 Columns in transition condition ($e=e_j$)**

Here, the transition condition represents that the RC column is set between large eccentric compression and small eccentric compression (i.e., the eccentricity $e$ equals the critical eccentricity $e_j$). In this case, the rebar on the far side of loading is in tension, while the rebar on the near side of loading is in compression. The failure mode of the rebar on the far side of loading depends on the bond effectiveness. According to the bond effectiveness of the rebar on the far side of loading, the following two cases should be considered.

***Case with effective bond ($e=e_j$)***

When the bond strength of the rebar on the far side of loading is effective, the stress-strain relationship between the rebar and the surrounding concrete is approximately consistent. The residual bearing capacity of the rebar on the far side of loading $F_{sx}$ is determined by the residual cross-sectional area $A_{sc}$ and the residual yield strength $f_{yc}$, defined in Eq. (1). Meanwhile, the rebar on the near side of loading may yield under compression, and its bearing capacity $F_{szx}$ is governed by the smaller value of yield strength $f'_{yc}$ and buckling strength $f_{cr}$, calculated from Eq. (25). From Figure 4(c), the strains of the rebar on the near side of loading $\varepsilon_{szx}$ and the rebar on the far side of loading $\varepsilon_{sx}$ can be obtained from the concrete strain $\varepsilon_c$ on the basis of the compatibility condition, expressed here as

$$\varepsilon_{sx} = \varepsilon_c \frac{h_0 - x_c - Y_x(X)}{Y_x(X)} \tag{30}$$

$$\varepsilon_{szx} = \varepsilon_c \frac{Y_x(X) + x_c - a'_s}{Y_x(X)} \tag{31}$$

By considering the bearing capacity of the rebar and the stress-strain relationship between the rebar and the surrounding concrete, the compression zone height of the concrete cross-section $Y_{xj}(X)$ under transition condition with the effective bond of rebar can be obtained from

$$Y_{xj}(X) = \frac{min(f'_{yc}, f_{cr})(h_0 - x_c) - f_{yc}(x_c - a'_s)}{min(f'_{yc}, f_{cr}) + f_{yc}} \tag{32}$$

***Case with bond degradation ($e=e_j$)***

When rebar corrosion reaches a high level, rebar anchorage failure occurs before the tensile rebar yields, leading to the incompatibility of the stress-strain relationship between the tensile rebar and the surrounding concrete. Meanwhile, rebar bond degradation has little effect on the compressive steel bars, as shown in Figure 4(d). The new deformation

compatibility equation between the tensile rebar and the surrounding concrete can be obtained by introducing the interpolation factor $G(X)$, namely $\varepsilon_{sc}=\varepsilon_{sx}/G(X)$. Based on the stress states of rebar, the bearing capacity of the rebar on the far side of loading, $F_{sx}$, is governed by the residual bond strength given by Eq. (21), and the residual bearing capacity of the rebar on the near side of loading, $F_{szx}$, can be calculated by Eq. (25). From Figure 4(d), the stress-strain relationship between the rebar and the concrete on the near side of loading is defined in Eq. (31), and the stress-strain relationship between the rebar on the far side of loading $\varepsilon_{sx}$ and the concrete $\varepsilon_c$ is rewritten here as

$$\varepsilon_{sx}=\frac{F_{ux}}{A_{sc}E_s}=\frac{\varepsilon_{sc}}{G(X)}=G(X)\varepsilon_c\frac{h_0-x_c-Y_x(X)}{Y_x(X)} \tag{33}$$

where $G(X)=\dfrac{gY_x(X)}{L_{ub}}$, in which $g=\dfrac{2(\varepsilon_{end}-\varepsilon_{start})}{\tan 17.5^{\circ}\,\varepsilon_{end}}$. When the rebar bond degrades, the critical compression zone height of the concrete cross-section $Y_{xj}(X)$ under the transition condition can be expressed as

$$A_1Y_{xj}(X)^2+B_1Y_{xj}(X)+C_1=0 \tag{34}$$

where parameters $A_1$, $B_1$, and $C_1$ are defined as $A_1=g\min(f_{cr},f_{yc}^{'})A_{sc}$, $B_1=F_{ux}L_{ub}-g(h_0-x_c)\min(f_{cr},f_{yc}^{'})A_{sc}$, and $C_1=F_{ux}L_{ub}(x_c-a_s^{'})$, respectively.

By substituting the concrete compression zone height $Y_{xj}(X)$ into Eqs. (29a) and (29b), the eccentricity $e_j$, axial force $N_j$ and bending moment $M_j$ under the transition condition can be calculated. The eccentricity $e_j$ can then be used to determine whether the corroded column is under large eccentric compression or small eccentric compression. When the eccentricity $e$ is greater than the critical eccentricity $e_j$ ($e>e_j$), the column is under large eccentric loading. In the case of $e<e_j$, the structure is under small eccentric loading. The residual load capacity for these two load cases are discussed below in detail.

**4.2.2 RC columns with small eccentricity ($e<e_j$)**

In the case of RC columns with small eccentricity ($e<e_j$), the rebar on the near side of loading yields under compression, and the rebar on the far side of loading may be in tension or compression. In order to fully understand the stress state of the rebar on the far side of loading, the bearing capacity of the rebar can be assumed here as $F_{sx}=0$, and the compression

zone height of the concrete cross-section can be defined as $Y_x(X)=h_0-x_c$. The critical eccentricity of RC column with small eccentricity $e_{sj}$ can then be calculated from

$$e_{sj}=\frac{a_1\beta_1 b_c f_c(h_0-x_c)(h_0-x_c-\beta_1(h_0-x_c)/2)+F_{szx}(h_0-a_s^{'})}{a_1\beta_1 b_c f_c(h_0-x_c)+F_{szx}}-h/2+a_s \tag{35}$$

***Case with 0<e<$e_{sj}$***

In the case with $0<e<e_{sj}$, the rebar on the far side of loading is in compression. The stress-strain relationship between the rebar on the far side of loading $\varepsilon_{sx}$ and the rebar on the near side of loading $\varepsilon_{szx}$ can be defined as

$$\varepsilon_{sx}/\varepsilon_{szx}=\frac{Y_x(X)+x_c-h_0}{Y_x(X)+x_c-a_s^{'}} \tag{36}$$

Based on the stress state of the rebar, the bearing capacity of the rebar on the near side of loading $F_{szx}$ can be calculated from Eq. (25), and the bearing capacity of the rebar on the far side of loading $F_{sx}$ can be obtained from the stress-strain relationship, expressed here as

$$F_{sx}=\min(f_{cr},f_{yc}^{'})A_{sc}\frac{Y_x(X)+x_c-h_0}{Y_x(X)+x_c-a_s^{'}} \tag{37}$$

Furthermore, the compression zone height of the concrete cross-section $Y_x(X)$ for the case with $0<e<e_{sj}$ can be obtained from

$$A_2Y_x(X)^3+B_2Y_x(X)^2+C_2Y_x(X)+D_2=0 \tag{38}$$

where parameters $A_2$, $B_2$, $C_2$, and $D_2$ are defined as $A_2=\frac{a_1\beta_1^2 f_c b_c}{2}$,

$B_2=a_1\beta_1 f_c b_c(\mathrm{e}_s-h_0+x_c+\frac{\beta_1 x_c}{2}-\frac{\beta_1 a_s^{'}}{2})$,

$C_2=a_1\beta_1 f_c b_c(e_s-h_0+x_c)(x_c-a_s^{'})+F_{szx}(e_s-h_0+a_s^{'})+\min(f_{cr},f^{'}_{yc})A_{sc}e_s$,

and $D_2=F_{szx}(e_s-h_0+a_s^{'})(x_c-a_s^{'})-\min(f_{cr},f^{'}_{yc})A_{sc}e_s(h_0-x_c)$, respectively.

***Case with $e_{sj}$<e<$e_j$***

In the case with $e_{sj}<e<e_j$, the rebar on the near side of loading yields under compression, as defined in Eq. (25), while the rebar on the far side of loading is in tension. The effect of the rebar bond strength degradation on the tensile rebar needs to be considered. When rebar bond is effective, the deformation compatibility between the rebar and the surrounding concrete is satisfied. Thus, the strains of the rebar on the near side of loading $\varepsilon_{szx}$ and the rebar on the far side of loading $\varepsilon_{sx}$ can be calculated from Eqs. (30) and (31), respectively. Based on the

stress-strain relationship, the residual bearing capacity of the rebar on the far side of loading $F_{sx}$ can be obtained from

$$F_{sx} = \min(f_{cr}, f_{yc}^{'}) A_{sc} \frac{h_0 - x_c - Y_x(X)}{Y_x(X) + x_c - a_s^{'}} \tag{39}$$

and the compression zone height of the concrete cross-section $Y_x(X)$ can be estimated from Eq. (38).

When rebar bond degrades, the deformation between the rebar on the far side of loading and the surrounding concrete is incompatible. The bond strength interpolation factor $G(X)$ is introduced here to obtain a new deformation compatibility between the tensile rebar and the surrounding concrete. The strains of the rebar on the near side of loading $\varepsilon_{szx}$ and the rebar on the far side of loading $\varepsilon_{sx}$ can be estimated by Eqs. (31) and (33), respectively. Thus, the bearing capacity of the rebar on the far side of loading $F_{sx}$ is rewritten here as

$$F_{sx} = G(X) \min(f_{cr}, f_{yc}^{'}) A_{sc} \frac{h_0 - x_c - Y_x(X)}{Y_x(X) + x_c - a_s^{'}} \tag{40}$$

In addition, the compression zone height of the concrete cross-section $Y_x(X)$ can be estimated from

$$A_3 Y_x(X)^3 + B_3 Y_x(X)^2 + C_3 Y_x(X) + D_3 = 0 \tag{41}$$

where parameters $A_3$, $B_3$, $C_3$, and $D_3$ are defined as $A_3 = \frac{a_1 \beta_1^2 f_c b_c}{2}$,

$$B_3 = a_1 \beta_1 f_c b_c (e_s - h_0 + x_c + \frac{\beta_1 x_c}{2} - \frac{\beta_1 a_s^{'}}{2}) + \frac{g \min(f_{cr}, f^{'}_{yc}) A_{sc} e_s}{L_{ub}},$$

$$C_3 = a_1 \beta_1 f_c b_c (e_s - h_0 + x_c)(x_c - a_s^{'}) + F_{szx}(e_s - h_0 + a_s^{'}) - \frac{g \min(f_{cr}, f^{'}_{yc}) A_{sc} e_s}{L_{ub}} (h_0 - x_c),$$

and $D_3 = F_{szx}(e_s - h_0 + a_s^{'})(x_c - a_s^{'})$, respectively.

### 4.2.3 RC columns with large eccentricity ($e>e_j$)

For the cases with $e>e_j$, the corroded column is under large eccentric compression. On the basis of the stress-strain diagram in Figure 4, the strain of the rebar on the near side of loading $\varepsilon_{szx}$ can be calculated from the ultimate concrete compressive strain $\varepsilon_{cu}$, expressed as

$$\varepsilon_{szx} = \varepsilon_{cu} \frac{x_c + Y_x(X) - a_s^{'}}{Y_x(X) + x_c} \tag{42}$$

The residual bearing capacity of the rebar on the far side of loading $F_{sx}$ is governed by the smaller value of the residual yield strength $f_{yc}$ and the residual bond strength $\tau_{ux}$. The

residual capacity of the rebar on the near side of loading $F_{szx}$ can be estimated from the stress-strain relationship, defined as, respectively

$$F_{sx} = \min(F_{sc}, F_{ux}) \tag{43}$$

$$F_{szx} = \min(\varepsilon_{cu} E_{sc} A_{sc}^{'} \frac{Y_x(X) + x_c - a_s^{'}}{Y_x(X) + x_c}, F_{sc}^{'}, F_{cr}) \tag{44}$$

where the buckling capacity of the corroded rebar $F_{cr}$ can be calculated from $F_{cr}=f_{cr}A_{sc}$, and $E_{sc}$ is the elastic modulus of the corroded longitudinal bars. The height of the concrete compression zone $Y_x(X)$ can be determined by the equilibrium condition of the resultant forces acting on the corroded column, as shown in Figure 4, expressed as

$$A_4 Y_x(X)^3 + B_4 Y_x(X)^2 + C_4 Y_x(X) + D_4 = 0 \tag{45}$$

where parameters $A_4$, $B_4$, $C_4$, and $D_4$ are defined as $A_4 = \frac{a_1 \beta_1^2 f_c b_c}{2}$, $B_4 = a_1 \beta_1 f_c b_c (e_s + x_c - h_0 + \frac{\beta_1 x_c}{2})$, $C_4 = a_1 \beta_1 f_c b_c x_c (e_s - h_0 + x_c) - F_{sx} e_s + \varepsilon_{cu} E_{sc} A_{sc}^{'} (e_s - h_0 + a_s^{'})$, and $D_4 = \varepsilon_{cu} E_{sc} A_{sc}^{'} (e_s - h_0 + a_s^{'})(x_c - a_s^{'}) - F_{sx} e_s x_c$, respectively.

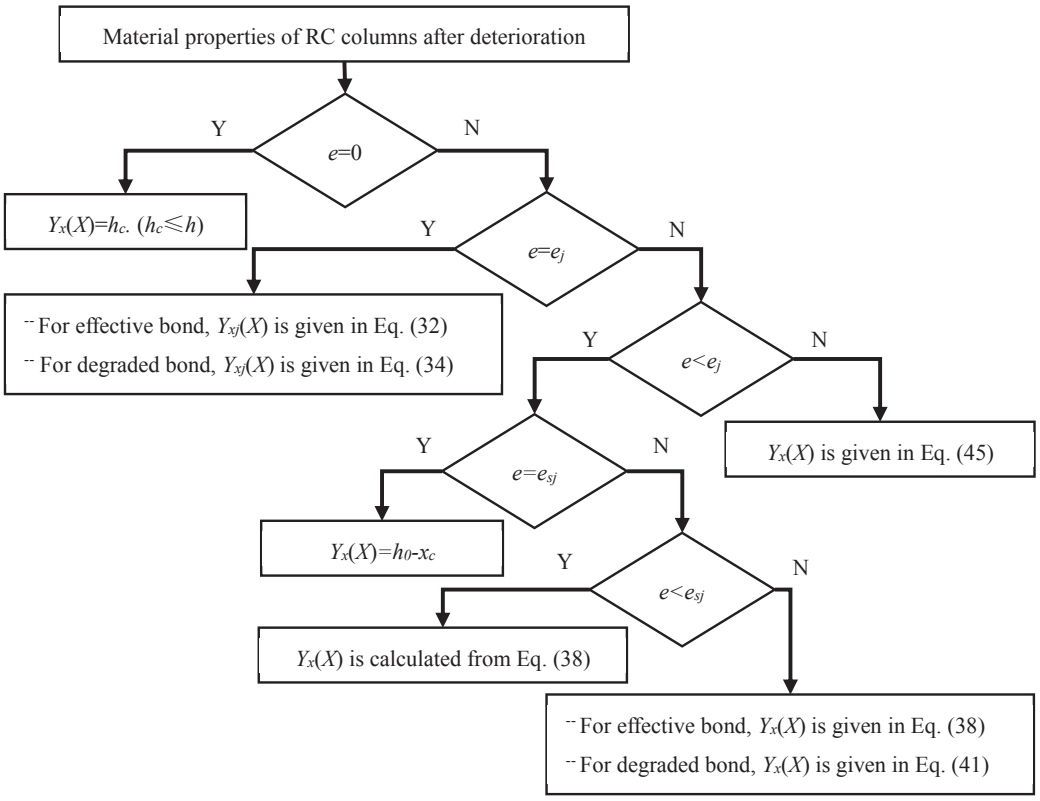


**Figure 5** Flow chart for determining residual bearing capacity of corroded RC columns

Consequently, the residual bearing capacity of the corroded columns under loading conditions discussed above can be obtained from Eqs. (29a, b). Figure 5 shows the flow chart for the computational procedure for determining the residual bearing capacity of the corroded columns.

## 5. Numerical example

A typical corrosion-affected RC column, described in Wang and Liang (2008), is now used to demonstrate the effectiveness of the proposed models. In the given experiments, partially corroded RC columns under eccentric loading were investigated, where the partially corroded lengths $L_{ub}$ were 350mm and 700mm, respectively, and the eccentric distances of 150 mm and 50 mm were chosen for the corroded RC columns to represent the applied load with large and small eccentricities, respectively. The design details of the corroded RC columns tested by Wang and Liang (2008) are shown in Figure 6.

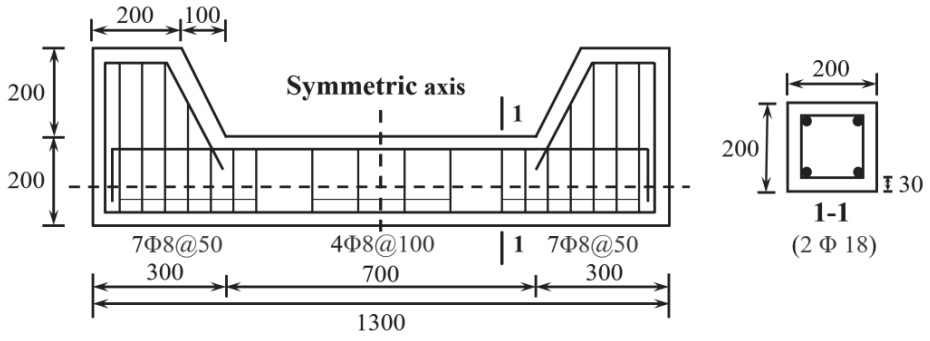


**Figure 6** Design details of the corroded RC columns tested by Wang and Liang (2008) (dimensions in mm)

The specimens had a length of $l$=1300 mm, with a rectangular cross-section of height $h$=200 mm and width $b$=200 mm. Two steel bars of a diameter of 18 mm were embedded into the far and near sides of loading, respectively, with the yield strength of $f_{y0}$=397.5 MPa and the modulus of elasticity $E_s$ =200 GPa. The stirrups consisted of the plain steel bars with a diameter of 8 mm, spacing at 100 mm in the central part. The concrete columns had an average clear cover thickness of 30 mm, with average actual compressive strength of $f_c$=41.5 MPa. By assuming that the loading point during the test is accurate with uniform material

quality, the additional eccentricity can be ignored, taken as $e_a$=0. The tested RC columns were considered as short ones with the assumption of no initial imperfection for compression, and the second-order effect on the RC column was ignored.

The material deterioration and structural strength degradation models proposed in this paper were employed for the tested RC columns. According to the test data, the parameters required for the proposed models were estimated by using the relevant methods (CEB-FIP, 1990; Zhang et al., 2009), as shown in Table 1.

**Table 1** Estimated parameters of concrete material.

| Parameter | Symbol | Evaluation | Value |
|---|---|---|---|
| Tensile strength | $f_t$ | $0.69(f_c)^{1/2}$ | 4.45MPa |
| Design bond strength | $f_{bd}$ | $0.315(f_c)^{0.67}$ | 3.82MPa |
| Modulus of elasticity | $E_c$ | $4400(f_c)^{0.516}$ | 30.09GPa |
| Fracture energy | $G_f$ | $G_{f0}(f_{cm}/f_{cm0})^{0.7}$ | 81.24N/m |
| Ultimate crack width | $w_u$ | $a_f G_f/f_t$ | 0.13mm |
| Critical crack width | $w_{cr}$ | $kG_f/f_c$ | 0.05mm |
| Total number of the cracks | $n_c$ | $2\pi R_c/L_c$ | 4 |

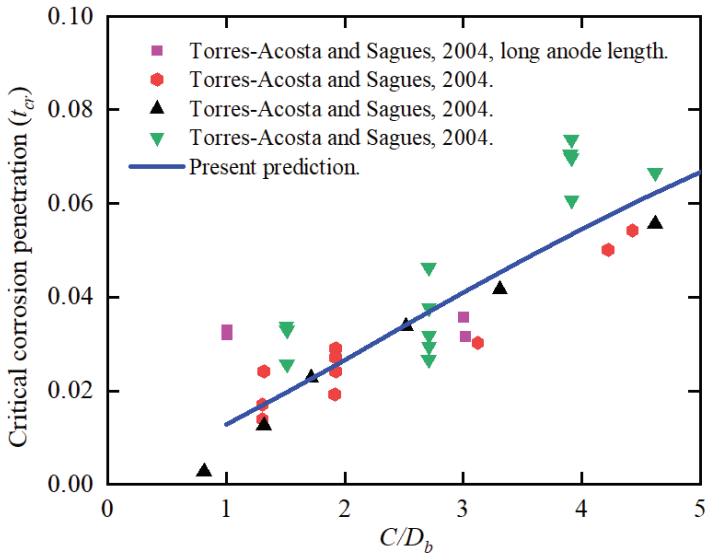


**Figure 7** Rebar critical corrosion penetration $t_{cr}$ as a function of concrete cover-to-rebar diameter ratio $C/D_b$, compared with available experimental data

Figure 7 shows the relationship between the critical corrosion penetration $t_{cr}$ and the concrete cover-to-rebar diameter ratio, $C/D_b$. The predicted results for the critical corrosion penetration are obtained from Eq. (6) and compared with the test results from Torres-Acosta and Sagues (2004) due to lack of data in the experiments. It can be found that the predicted results from the proposed models are in good agreement with experimental data, and the relationship between the critical corrosion penetration and the concrete cover-to-rebar diameter ratio shows a positive linear correlation law.

Figure 8 shows the predicted equivalent crack width on the concrete cover surface $w_c$ as a function of rebar corrosion level $X$ (%), as defined in Eq. (14), in which the volume expansion factor $\xi_r$ is taken here as 2. From the results, the crack width grows as corrosion level increases, matching well with the experimental data from various sources (Alonso et al.,1998; Vidal et al., 2004; Coronelli et al., 2013; Banba et al., 2014; Khan et al., 2014). When the corrosion level reaches approximately 1%, the cracks appear on the concrete cover surface, and the predicted equivalent crack width reaches 1.1mm at corrosion level of 15%.

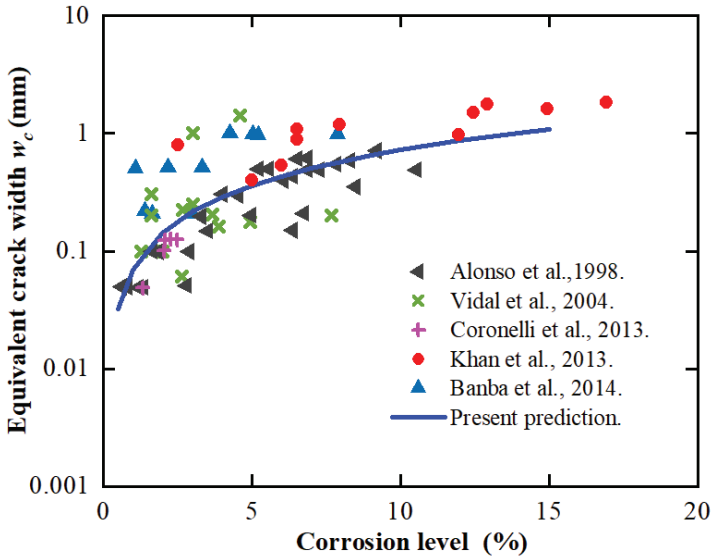


**Figure 8** Predicted equivalent crack width $w_c$ (mm) versus rebar corrosion level $X$ (%), compared with experimental data available from various sources

The degradation of rebar bond strength is evaluated from Eq. (20) as a function of the equivalent crack width on the concrete cover surface $w_c$, where coefficient $\lambda_\eta$ is taken here as

20 (Cairns et al., 2006), as shown in Figure 9. The residual bond strength of the corroded rebar has a strong relationship with the concrete crack width, and the predicted results are in good agreement with the experimental data from existing studies (Rodriguez et al., 1994; Fischer, 2010; Law et al., 2011; Li and Yuan, 2013). The rebar bond strength starts decreasing at the appearance of cracks on the concrete surface, then reduces significantly at the early stage of cracks propagation, and finally maintains a small value as concrete crack width becomes relatively large.

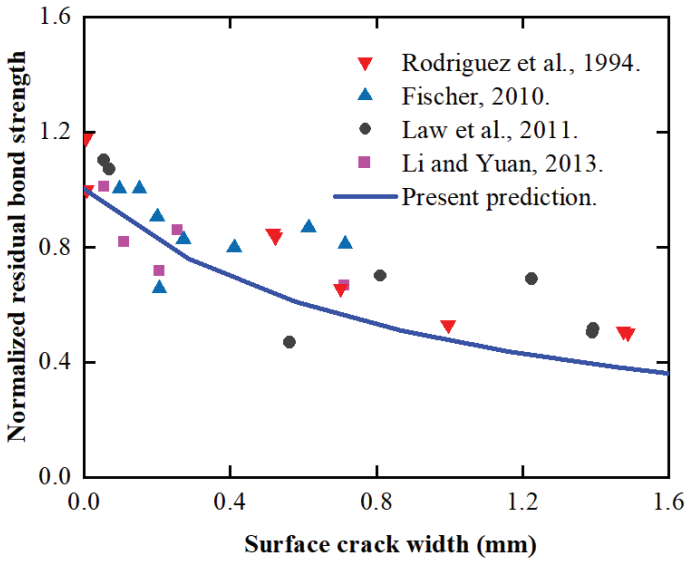


**Figure 9** Predicted normalized residual bond strength versus cover surface crack width, compared with experimental data available from various sources

Based on the predicted results of the concrete crack width growth and the rebar bond strength degradation, the evolution of the column concrete compression zone height was investigated to accurately evaluate the residual bearing capacity of the corroded RC column, as shown in Figure 10. The results showed that the compression zone height of the concrete column cross-section decreases with an increase in corrosion level. When the corrosion level of rebar reaches 20%, the concrete compression zone height reduces to 69.50%, 66.33%, 54.32%, 30.87% and 29.52% for the eccentricities of $e$=0.00m, 0.02m, 0.05m, 0.10m, and 0.15m, respectively. When corrosion level ranges from 5% to 10%, the height of the concrete

compression zone decreases significantly, mainly due to the degradation of the rebar bond strength and the reduction of the concrete cross-sectional area.

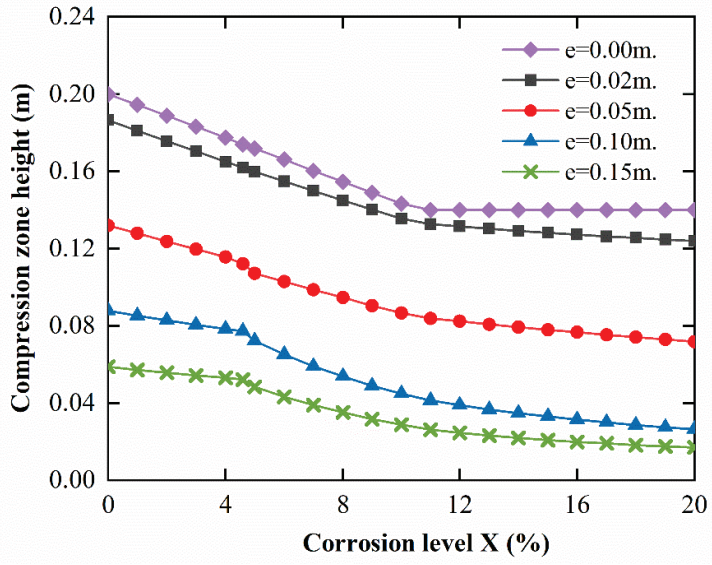


**Figure 10** Change of the concrete compression zone height of RC columns with various eccentricities as a function of rebar corrosion level

In Table 2, the residual load capacity of the corroded RC columns was calculated from the proposed models and compared with the experimental results in Wang and Liang (2008). From the calculated results, the relative error $(N_{cal}\text{-}N_{exp})/N_{exp}$ ranges from -0.075 to 0.174, with a mean absolute value of 0.073 and a variance of 0.0052. In general, the predicted results are slightly larger than the test results, which is probably affected by the inaccurate measurement of loading point and the variation of concrete compressive strength. The predicted results are in good agreement with the experimental results, which demonstrates the effectiveness of the proposed models.

**Table 2** Comparison of the predicted residual load capacity of the corroded RC column with experimental data available.

| NO. | Specimen | b×h (mm) | $f_c$ (MPa) | | $e$ (mm) | $X_{max}$ (%) | | $N_{exp}$ (KN) | $N_{cal}$ (KN) | Relative error |
|---|---|---|---|---|---|---|---|---|---|---|
| | | | $f_{c\text{-}cor}$ | $f_{c\text{-}unc}$ | | Far | Near | | | |
| (1) | ZD0 | 203×185 | - | 36.0 | 156.5 | 0.00 | 0.00 | 239.1 | 269.0 | 0.125 |
| (2) | ZDL700-1 | 201×201 | 38.4 | 43.1 | 149.5 | 1.85 | 2.54 | 255.3 | 265.3 | 0.039 |
| (3) | ZDL700-2 | 208×190 | 40.0 | 45.3 | 155.0 | 5.14 | 3.02 | 232.8 | 248.4 | 0.067 |
| (4) | ZDL350-3 | 205×201 | 40.0 | 45.3 | 150.5 | 4.38 | 4.31 | 240.1 | 254.8 | 0.061 |
| (5) | ZDY700-1 | 200×198 | 38.4 | 43.1 | 150.0 | 1.01 | 4.89 | 269.2 | 249.0 | -0.075 |
| (6) | ZDY350-2 | 204×192 | 40.0 | 45.3 | 152.0 | 1.00 | 3.94 | 223.9 | 239.6 | 0.070 |
| (7) | ZXY700-1 | 205×195 | 40.0 | 45.3 | 53.5 | 0.00 | 2.42 | 741.2 | 870.3 | 0.174 |
| (8) | ZXY350-2 | 204×200 | 40.0 | 45.3 | 53.9 | 1.62 | 5.59 | 696.5 | 657.5 | -0.056 |
| (9) | ZXY350-3 | 204×204 | 40.0 | 45.3 | 46.0 | 4.92 | 8.45 | 613.1 | 608.5 | -0.007 |
| (10) | ZXL700-1 | 206×198 | 38.4 | 43.1 | 51.0 | 2.14 | 4.32 | 756.5 | 798.6 | 0.056 |

Figure 11 shows the predicted results for the residual bearing capacity of the corroded columns as a function of rebar corrosion level, and the predicted results are then compared with the experimental data in Wang and Liang (2008). The residual load-carrying capacity of the corroded columns was estimated with two cases considered, i.e. intact bond strength and bond strength damaged by rebar corrosion. The results predicted by the proposed models with consideration of bond strength degradation are in a better agreement with the experimental data, compared with results for the case with intact rebar bond. From Figure 11, in the case with corrosion level less than 5%, the residual bearing capacity is very close to each other for the intact and degraded bond conditions, since the bond strength loss has little effect on the bearing capacity of the RC column in this case. When the corrosion level exceeds 5%, the difference appears between the intact and degraded bond conditions, and increases gradually with the corrosion level growth. When rebar corrosion level reaches 20%, the residual capacity for the case with bond degradation reduces to 94.68%, 64.33%, and 52.55% of that for the case with intact bond for the eccentricity of $e$=0.05m, 0.1m, and 0.15m, respectively. Thus, the influence of rebar bond strength degradation on the residual bearing capacity of the corroded columns can be significant and should not be ignored.

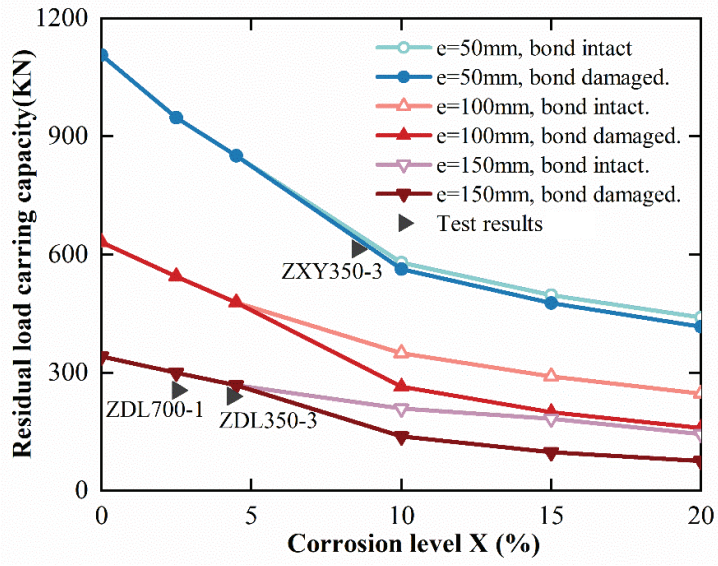


**Figure 11** Predicted residual bearing capacity of corroded RC columns with or without influence of rebar bond degradation, compared with test results in Wang and Liang (2008)

From the results obtained above, the moment-axial force (M-N) interaction curves of the corroded RC column with three damage cases were investigated, i.e., corrosion damage at the rebar on the far side of loading, at the rebar on the near side of loading, and in all rebar. The moment-axial force (M-N) interaction curves given by the proposed method are then compared with the experimental data in Wang and Liang (2008) and the calculated results from Tapan and Aboutaha (2011).

Figure 12 shows the results for the M-N interaction diagram at various corrosion levels from the proposed method for the case with corrosion damage at the rebar on the far side of loading. The obtained results of the M-N interaction diagram are closer to the experimental data in Wang and Liang (2008) than the results in Tapan and Aboutaha (2011), which is mainly due to the improved models of the rebar bond strength degradation proposed in this paper. From the results, the residual bearing capacity of the corroded column under axial compression ($e$=0) and small eccentric compression ($e<e_j$) has a relatively low reduction. When corrosion level is in the range of 5-10%, the residual capacity of the corroded RC column with large eccentricity ($e>e_j$) drops significantly due to the deterioration of the rebar bond strength and the reduction in the height of the concrete compression zone.

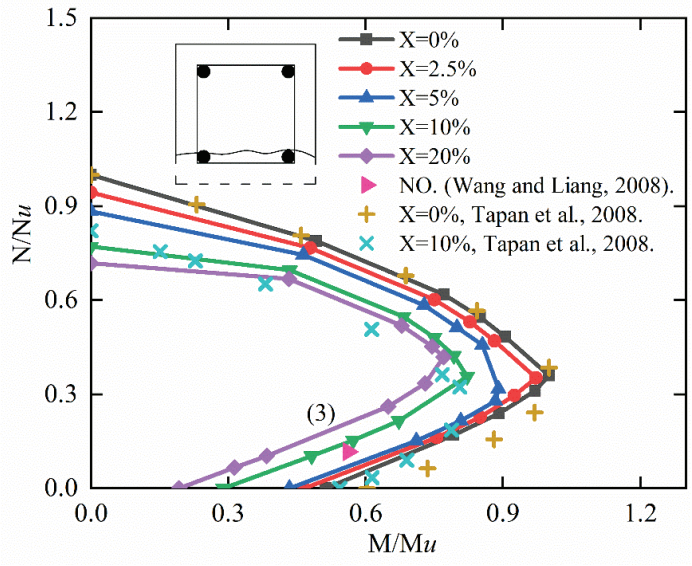


**Figure 12** M-N interaction diagram for the corroded RC column, where rebar corrosion occurs on the side away from the load

Figure 13 presents the results for the M-N interaction diagram at various corrosion levels for the case with corrosion damage at the rebar on the near side of loading. The obtained results of the M-N interaction diagram are in a better agreement with the experimental data, comparing the results given in Tapan and Aboutaha (2011). This is mainly due to the consideration of the concrete cross-sectional area reduction and the concrete compression zone height change in the proposed models. The residual capacity of the corroded column under axial load ($e$=0) and small eccentric compression ($e<e_j$) reduces significantly in this case, which is mainly caused by the loss of concrete cover on the near side of loading, the reduction in the compression zone height of the concrete cross-section, and the buckling of the corroded rebar. On the other hand, the load-carrying capacity of the corroded RC column with large eccentricity decreases relatively slowly.

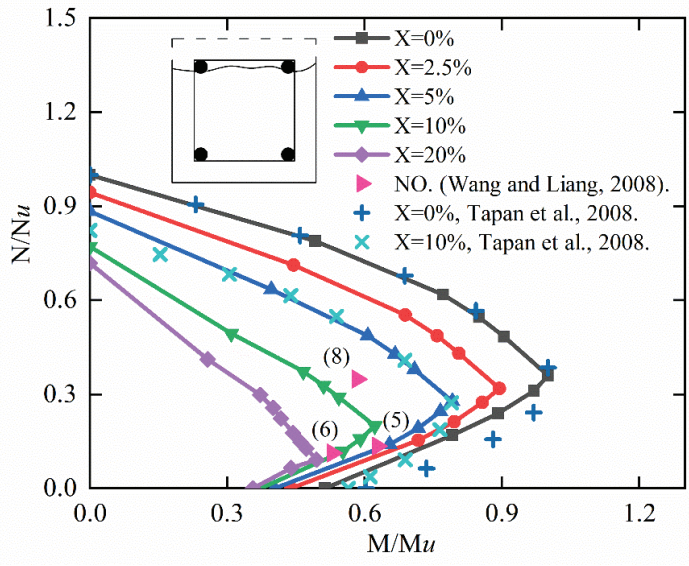


**Figure 13** M-N interaction diagram for the corroded RC column, where rebar corrosion occurs on the side close to the load

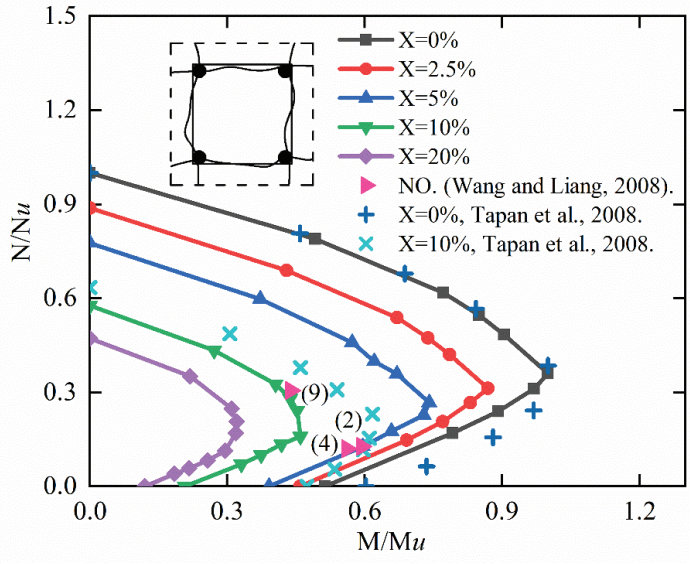


**Figure 14** M-N interaction diagram for the corroded RC column, where rebar corrosion occurs on all sides

Figure 14 gives the results of the M-N interaction diagram at various corrosion levels for the case with corrosion damage in all steel bars. The results of the M-N interaction diagram obtained from the proposed models appear better agreement with the existing experimental data, due to the application of the improved models proposed in this study. From the results, the bearing capacity of the corroded RC column under axial compression ($e$=0) and small

eccentricity compression ($e<e_j$) decreases significantly at the corrosion level between 5-10%, which is mainly caused by the loss of the concrete cross-section and the decrease in the concrete compression zone height. The residual capacity of the corroded column with large eccentric compression ($e>e_j$) also reduces obviously, when corrosion level ranges between 5-10%. Moreover, the rebar corrosion may transfer the structural failure mode of the RC column from large eccentric compression failure to small eccentric compression failure.

The structural failure risk in corrosive environments depends upon the corrosion rate $i_{corr}$. The service life of the corroded RC columns with different eccentricities, i.e., $e$=0.05m and 0.15m, was predicted by considering various corrosion rates of $i_{corr}$=0.3$uA/cm^2$, 1$uA/cm^2$ and 3$uA/cm^2$, corresponding to low, moderate and high corrosion rates, respectively. Here, the normalized load capacity is defined as the ratio of the residual bearing capacity of the corroded column to that of the original column, and it is assumed that the RC structure fails where the residual bearing capacity is less than 70% of the original structure.

Figure 15 shows the results for the service life of the corroded RC column in different corrosive environments with an eccentricity of $e$=0.05mm. Here, the service life of the column in a low-risk corrosive environment exceeds 75 years, but decreases to 23 years in a moderate-risk corrosive environment. The service life of the structure has a significant reduction with a value of approximately 8 years in a highly corrosive environment.

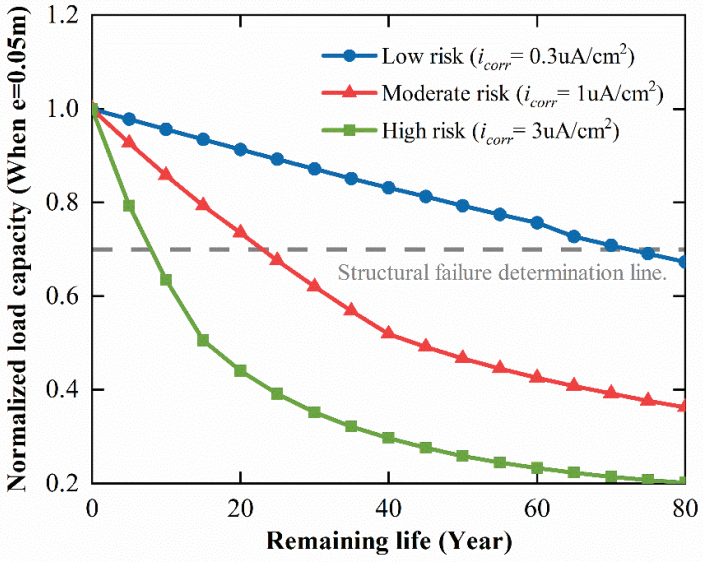


**Figure 15** Predicted service life of the corroded RC column ($e$ =0.05m) in various corrosive environments

From the results in Figure 16, the service life of the RC column with an eccentricity of $e$ =0.15m in a low-risk corrosive environment reaches 75 years, but reduces to 22 years in a moderate-risk corrosive environment. Here again, the corroded RC column has a significantly reduced service life of only about 7 years in a high-risk corrosive environment.

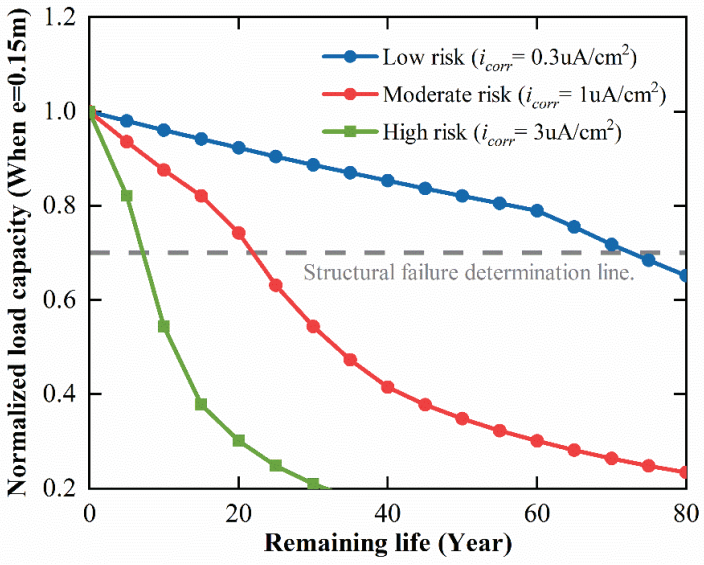


**Figure 16** Predicted service life of the corroded RC column ($e$ =0.15m) in various corrosive environments

From the results in Figures 15-16, the corrosive environment has a significant effect on the service life of the corroded RC structures. Therefore, it is necessary to take effective maintenance and repair measures for the corroding RC structures in severe corrosive environments, especially at the early stage of rebar corrosion.

## 6. Conclusions

This paper investigated the structural performance deterioration of RC columns caused by rebar corrosion, and provided new analytical models for predicting the residual bearing capacity of the corroded RC columns in aggressive environments. The material deterioration models and structural strength degradation models were constructed, and then the load-carrying capacity of the corroded RC columns was estimated for various cases of rebar corrosion locations and loading conditions. The M-N interaction diagrams of the corroded

RC columns under varying corrosion levels were obtained, and the service life of the corroded RC columns in different corrosive environments was also investigated. Finally, a numerical example was adopted to demonstrate the effectiveness of the proposed models, and the predicted results agreed well with the experimental data available from various sources. On the basis of the results obtained from the numerical example, the following conclusions could be drawn:

**1)** The residual bearing capacity of the corroded RC columns can be significantly affected by many factors, such as rebar corrosion level, rebar bond strength degradation, concrete cover cracking and spalling, and change in the compression zone height of the concrete cross-section.

**2)** The loading condition of the corroding RC columns also has a significant effect on the residual bearing capacity of the columns. At relatively high rebar corrosion level, the bearing capacity of the corroded RC columns decreases obviously for the cases under axial compression and small eccentric compression, mainly due to the reduction of concrete cross-sectional area, however in the case with large eccentricity, the main cause is changed to rebar bond loss.

**3)** The service life of the corroded RC columns largely depends on the operation environments, and can be reduced remarkably in a high-risk corrosive condition. The significant reduction of the bearing capacity of the corroded RC columns generally occurs at the early corrosion stage, thus effective maintenance and repair measures are necessary for the corroding RC structures. Furthermore, the maintenance strategy of the corroded RC structures should be optimised by using the time-dependent reliability analysis and the lifetime cost analysis, and the combined action of load and aggressive environment should be considered for structural performance deterioration predictions in further studies.

**Acknowledgements**

The authors are very grateful for the financial supports received from the National Key Research and Development Program of China (Grant No. 2021YFE0105600), the National Natural Science Foundation of China (Grant No. 51978263) and the Key Project for

Scientific and Technological Cooperation Scheme of Jiangxi Province (Grant No. 20212BDH80022).

## References

Alonso, C., Andrade, C., Rodriguez, J., et al., 1998. Factors controlling cracking of mortar affected by reinforcement corrosion. Mater. Struct. 31, 435-441. https://doi.org/10.1007/bf02480466.

Andrade, C., Garcés, P., Baeza, F.J., et al., 2015. Electronic and Electrolytic Conduction of Cement Pastes with Additions of Carbonaceous Materials, In Andrade, C., Gulikers, J., Polder, R., Durability of Reinforced Concrete from Composition to Protection, Springer: Cham (ZG), Switzerland. pp. 11-25. https://doi.org/10.1007/978-3-319-09921-7.

Balestra, C.E.T., Nakano, A.Y., Savaris, G., et al., 2019. Reinforcement corrosion risk of marine concrete structures evaluated through electrical resistivity: Proposal of parameters based on field structures. Ocean Eng. 187, 106167. https://doi.org/10.1016/j.oceaneng.2019.106167.

Banba, S., Abe, T., Nagaoka, K., et al., 2014. Evaluation Method for Bond-Splitting Behavior of Reinforced Concrete with Corrosion Based on Confinement Stress of Concrete against Corrosion Expansion. J. Adv. Concrete Tech. 12 (1), 7-23. https://doi.org/10.3151/jact.12.7.

Cairns, J., Du, Y., Law, D., 2006. Residual bond strength of corroded plain round bars. Mag. Concr. Res. 58 (4), 221-231. https://doi.org/10 .1680/macr.2006.58.4.221.

CEB-FIP (Comité Euro-international du Béton-Fédération International de la Précontrainte), Design code. London: Thomas Telford. (1990).

Chen, H.P., 2018. Residual Flexural Capacity and Performance Assessment of Corroded Reinforced Concrete Beams. J. Struct. Eng. 144 (12). https://doi.org/10.1061/(asce)st.1943-541x.0002144.

Chen, H.P., Alani, A.M., 2013. Optimized Maintenance Strategy for Concrete Structures Affected by Cracking due to Reinforcement Corrosion. ACI Struc. J. 110 (2), 229-238. https://doi.org/10.14359/51684403.

Chen, H.P., Nepal, J., 2018. Modeling Residual Flexural Strength of Corroded Reinforced

Concrete Beams. ACI Struct. J. 115 (6), 1625-1635. https://doi.org/10.14359/51702232.

Chen, H.P., Xiao, N., 2012. Analytical Solutions for Corrosion-Induced Cohesive Concrete Cracking. J. Appl. Math. 2012, 1-25. https://doi.org/10.1155/2012/769132.

Chiu, C. K., Tu, F. J., Hs 文中 iao, F. P., 2014. Lifetime seismic performance assessment for chloride-corroded reinforced concrete buildings. Struct. Infrastruct. Eng., 11(3), 345–362. https://doi.org/10.1080/15732479.2014.886596.

Chung, L., Cho, S. H., Jay Kim, J. H., et al., 2004. Correction factor suggestion for ACI development length provisions based on flexural testing of RC slabs with various levels of corroded reinforcing bars. Eng. Struct. 26(8), 1013–1026. https://doi.org/10.1016/s0141-0296(04)00012-4.

Coccia, S., Imperatore, S., Rinaldi, Z., 2016. Influence of corrosion on the bond strength of steel rebars in concrete. Mat. and Struct. 49 (1-2), 537-551. https://doi.org/10.1617/s11527-014-0518-x.

Coronelli, D., Hanjari, K.Z., Lundgren, K., 2013. Severely Corroded RC with Cover Cracking. J. Struct. Eng. 139 (2), 221-232. https://doi.org/10.1061/(asce)st.1943-541x.0000633.

Dang, V.H., François, R., 2013. Influence of long-term corrosion in chloride environment on mechanical behaviour of RC beam. Eng. Struct. 48, 558-568. https://doi.org/10.1016/j.engstruct.2012.09.021.

Daniell, J.E., Cehlers, D.J., Griffith, M.C., et al., 2008. The softening rotation of reinforced concrete members. Eng. Struct. 30 (11), 3159-3166. https://doi.org/10.1016/j.engstruct.2008.04.023.

Dong, W., Ye, J.B., Murakami, Y., et al., 2016. Residual load capacity of corroded reinforced concrete beam undergoing bond failure. Eng. Struct. 127, 159-171. https://doi.org/10.1016/j.engstruct.2016.08.044.

Du, Y.G., Clark, L.A., Chan, A.H.C., 2005. Residual capacity of corroded reinforcing bars. Mag. Concrete Res. 57 (3), 135-147. https://doi.org/10.1680/macr.2005.57.3.135.

Fischer, C., 2010. Experimental investigations on the effect of corrosion on bond of deformed bars.

Ho, J., Kwan, A., Pam, H., 2004. Minimum flexural ductility design of high-strength concrete beams. Mag. Concr. Res. 56, 13-22. https://doi.org/10.1680/macr.56.1.13.36291.

Hui, Y.L., Li, R., Lin, Z.S., 1997. Experimental studies on the property before and after corrosion of rebars in basic concrete members. Industrial Construction. 27 (6), 14-18. (in Chinese) http://dx.chinadoi.cn/10.3321/j.issn:1000-8993.1997.06.004.

Khan, I., Francois, R., Castel, A., 2014. Prediction of reinforcement corrosion using corrosion induced cracks width in corroded reinforced concrete beams. Cem. Concr. Res. 56, 84-96. https://doi.org/10.1016/j.cemconres.2013.11.006.

Law, D.W., Tang, D., Molyneaux, T., et al., Structures, 2011. Impact of crack width on bond: confined and uneonfined rebar. Mat. and Struct. 44 (7), 1287-1296. https://doi.org/10.1617/s11527-010-9700-y.

Li, F., Yuan, Y., 2013. Effects of corrosion on bond behavior between steel strand and concrete. Constr. Build. Mater. 38, 413-422. https://doi.org/10.1016/j.conbuildmat. 2012.08.008.

Liang, Y.Q., Wang, L.C., 2020. Prediction of corrosion-induced cracking of concrete cover: A critical review for thick-walled cylinder models. Ocean Eng. 213. https://doi.org/10.1016/j.oceaneng.2020.107688.

Ma, Y., Che, Y., Gong, J., 2012. Behavior of corrosion damaged circular reinforced concrete columns under cyclic loading. Constr. Build. Mater. 29, 548-556. https://doi.org/10.1016/j.conbuildmat.2011.11.002.

Meda, A., Mostosi, S., Rinaldi, Z., 2014. Experimental evaluation of the corrosion influence on the cyclic behaviour of RC columns. Eng. Struct. 76, 112-123. https://doi.org/10.1016/j.engstruct.2014.06.043.

Rodriguez, J., Ortega, L.M., Casal, J., 1994. Corrosion of reinforcing bars and service life of reinforced concrete structures: Corrosion and bond deterioration. International Conference on Concrete Across Borders. 2, 315-326.

Saatcioglu, M., Razvi, S. R., 1992. Strength and Ductility of Confined Concrete. J. Struct. Eng. 118(6), 1590–1607. https://doi.org/10.1061/(asce)0733-9445(1992)118:6(1590).

Tapan, M., Aboutaha, R.S., 2011. Effect of steel corrosion and loss of concrete cover on strength of deteriorated RC columns. Constr. Build. Mater. 25 (5), 2596-2603. https://doi.org/10.1016/j.conbuildmat.2010.12.003.

Torres-Acosta, A.A., Sagues, A.A., 2004. Concrete cracking by localized steel corrosion - Geometric effects. ACI Mater. J. 101 (6), 501-507. https://doi.org/10.14359/13489.

Val, D., Chernin, L., Stewart, M., 2009. Experimental and Numerical Investigation of Corrosion-Induced Cover Cracking in Reinforced Concrete Structures. J. Struct. Eng. 135, 376-385. https://doi.org/10.1061/(asce)0733-9445(2009)135:4(376).

Vidal, T., Castel, A., Francois, R., 2004. Analyzing crack width to predict corrosion in reinforced concrete. Cem. Concr. Res. 34 (1), 165-174. https://doi.org/10.1016/s0008-8846(03)00246-1.

Wang, X.H., Liang, F.Y., 2008. Performance of RC columns with partial length corrosion. Comput. Concrete. 238 (12), 3194-3202. https://doi.org/10.1016/j.nucengdes.2008.08.007.

Wang, X.H., Liu, X.L., 2009. Predicting the flexural capacity of RC beam with partially unbonded steel reinforcement. Nucl. Eng. Des. 6 (3), 235-252. https://doi.org/10.1016/j.cemconres.2003.12.028.

Yalciner, D.D.H., Kumbasaroglu, D.D.A., Karimi, A., 2019. Prediction of Seismic Performance Levels of Corroded Reinforced Concrete Columns as a Function of Crack Width. Mater. Perfom. Charact. 3, 376-397. https://doi.org/10.1520/acem20190035.

Yalciner, H., Kumbasaroglu, A., 2020. Experimental Evaluation and Modeling of Corroded Reinforced Concrete Columns. ACI Mater. J. 117 (4), 61-76. https://doi.org/10.14359/51721372.

Yu, H.F., Da, B., Ma, H.Y., et al., 2017. Durability of concrete structures in tropical atoll environment. Ocean Eng. 135, 1-10. https://doi.org/10.1016/j.oceaneng.2017.02.020.

Yu, L.W., Francois, R., Dang, V.H., et al., 2015. Structural performance of RC beams damaged by natural corrosion under sustained loading in a chloride environment. Eng. Struct. 96, 30-40. https://doi.org/10.1016/j.engstruct.2015.04.001.

Zhang, K.J., Xiao, J.Z., Zhao, Y.X., et al., 2019. Analytical model for critical corrosion level of reinforcements to cause the cracking of concrete cover. Constr. Build. Mater. 223, 185-197. https://doi.org/10.1016/j.conbuildmat.2019.06.210.

Zhang, R.J., Castel, A., Francois, R., 2010. Concrete cover cracking with reinforcement corrosion of RC beam during chloride-induced corrosion process. Cem. Concr. Res. 40 (3), 415-425. https://doi.org/10.1016/jcemconres.2009.09.026.

Zhu, W.J., Francois, R., 2014. Corrosion of the reinforcement and its influence on the residual structural performance of a 26-year-old corroded RC beam. Constr. Build. Mater. 51, 461-472. https://doi.org/10.1016/j.conbuildmat.2013.11.015.